Influence of vibration mode and orientation of deformed nucleus on the deflection function in heavy ion reactions

D.P. Min

Tome 40 N° 5 MAI 1979

LE JOURNAL DE PHYSIQUE

Classification
Physics Abstracts
25.70

Influence of vibration mode and orientation of deformed nucleus on the deflection function in heavy ion reactions

D. P. Min

DPh-N/MF, CEN Saclay, B.P. 2, 91190 Gif sur Yvette, France

(*Reçu le 17 novembre 1978, révisé le 18 janvier 1979, accepté le 22 janvier 1979*)

Résumé. — Les réactions entre ions lourds sont étudiées dans le cadre de la mécanique classique à trois dimensions. L'un des noyaux est sphérique, l'autre sphéroïdal. Les vibrations du noyau sphéroïdal sont prises en compte. Il est montré que les variations de forme et d'orientation du noyau sphéroïdal ont une influence sensible sur la distribution angulaire et la polarisation des produits de réaction.

Abstract. — Heavy ion collisions are studied in the framework of three dimensional classical mechanics. One of the colliding nuclei is spherical, the other being spheroidal. The vibrations of the spheroidal nucleus are taken into account. It is shown that the variations of the shape and orientation of the spheroidal nucleus can have an appreciable influence on the angular distribution and the polarization of the reaction products.

1. **Introduction.** — Heavy ion interactions and in particular deep inelastic collisions, have been studied with the help of many models [1]. In most of these models, the deterministic character of classical mechanics is supplemented by the phenomenological introduction of statistical and thermodynamical considerations in order to describe the subsequent dispersion of such physical quantities as mass, charge, relative kinetic energy and spin.

It has been already shown by Deubler and Dietrich [1] that the inclusion of shape degrees was essential for obtaining the experimentally measured loss of translational energy. But it was then assumed that the classical trajectories were lying in a plane. As the first purpose of this work was to understand the de-orientation of the spin angular momentum observed in some experiments [2], collision has been described within the framework of three dimensional classical mechanics.

However, this three dimensional extension of the previous models has been restricted to the collision of a deformable spheroidal nucleus with a spherical nucleus. Large amplitude mass vibrations have been allowed, provided that they remained within the limit of spheroidal shapes.

Before entering into the model description and the results, we would like to emphasize that such elements as variations of the shape and orientation of deformed nucleus can have an appreciable influence on the angular distribution and the polarization of the reaction products, even though friction and nuclear vibrational damping are not taken into account in our model.

2. **Model.** — In order to characterize the system, the following collective degrees of freedom are taken into account dynamically :

i) The position vector of relative distance between two centres of mass (C.M.) of the nuclei ($\mathbf{r} = (r, \Theta, \Phi)$).

ii) The orientation of the symmetry axis of a spheroidal target nucleus by means of Euler angles ($\hat{\sigma} = (\varphi, \theta, \psi)$, where ψ does not specify the macroscopic shape of the spheroid because of its symmetry. From now on, $\hat{\sigma}$ will therefore be specified only by its components (θ, φ)).

iii) A shape coordinate for which we take the eccentricity (ε). ε is defined as follows for the spheroid $x^2/a^2 + y^2/a^2 + z^2/c^2 = 1$ in its body-fixed coordinate system,

$$\varepsilon = (c^2 - a^2)^{1/2}/c$$

which is real for the prolate shape ($1 > \varepsilon > 0$) and pure imaginary for the oblate shape ($\varepsilon = i\varepsilon'$, $\infty > \varepsilon' > 0$). In the figures, $-\varepsilon'$ is used instead of ε for convenience.

We assume that the nuclear flow inside the spheroidal nucleus has a vibrational velocity field $\mathbf{v}_0$ such as :

$$\text{rot } \mathbf{v}_0 = 0 .$$

We assume also that the nuclear fluid is incompressible.

Then

$$\operatorname{div} \mathbf{v}_0 = 0 .$$

When the whole nucleus rotates with an angular velocity $\boldsymbol{\omega}(t)$, the total velocity field at the point $\mathbf{r}_0$ is

$$\mathbf{v} = \mathbf{v}_0 + \boldsymbol{\omega} \times \mathbf{r}_0 .$$

This field verifies the following equations

$$\begin{cases} \nabla . \mathbf{v} = 0 \\ \nabla \times \mathbf{v} = 2\,\boldsymbol{\omega}(t) . \end{cases}$$

This mass fluid is therefore incompressible and rotational. The kinetic energy of the nucleus can be written :

$$T_d = \rho \int dV \mathbf{v}^2/2$$

$$= T_{vib} + T_{rot} + \boldsymbol{\omega} . \int dV \rho(\mathbf{r}_0 \times \mathbf{v}_0) \qquad (1)$$

$$T_{vib} = \rho \int dV \mathbf{v}_0^2/2 = \frac{1}{2} I_{vib}\, \varepsilon^2$$

$$T_{rot} = \rho \int dV (\boldsymbol{\omega}(t) \times \mathbf{r}_0)^2/2 = \frac{1}{2} \boldsymbol{\omega}(t) . \overleftrightarrow{I}_{rot} . \boldsymbol{\omega}(t) ,$$

where ρ is the nuclear density and the integration is taken over the whole volume of the nucleus. The third term of eq. (1) represents the coupling between rotation and vibration. Vibrational spin,

$$\int dV \rho(\mathbf{r}_0 \times \mathbf{v}_0) ,$$

is zero due to the symmetry of the spheroid. If this term were not zero, simple separation of vibration and rotation could be ambiguous. I_{vib} and the rotational moment of inertia I^1_{rot} about the axis perpendicular to the symmetry axis of the spheroid are shown in figure 1-1 as a function of ε. The Lagrangian of the system is

$$L = T - V$$

$$T = \frac{1}{2} \mu \dot{\mathbf{r}}^2 + T_{vib} + T_{rot}$$

$$V = V_N + V_Q + V_d ,$$

where μ is the reduced mass of the system.

Proximity nuclear potential (V_N) without any approximation is used [3]. A detailed discussion of the merits and validity restrictions usually made in similar calculations can be found in a recent paper by J. Randrup [4]. In figure 1-2 we show the mean curvature $\overline{R}$ as a function of ε, and it can be shown that V_N has a close affinity to the plotted $\overline{R}(\varepsilon)$ results. The exact Coulomb potential (V_Q) between the spheroid target and spherical projectile is deduced from reference [5].

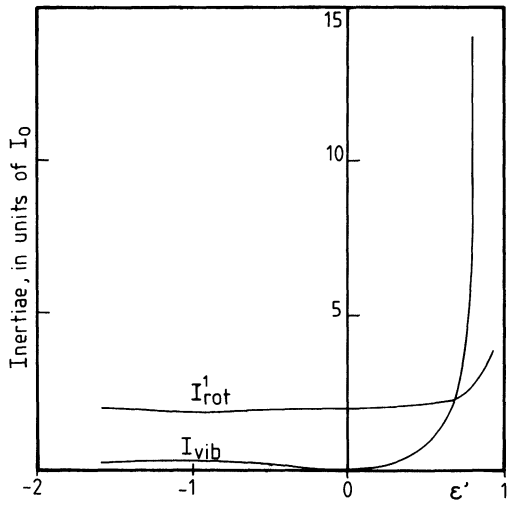

Fig. 1-1. — Model calculation of vibrational inertia (I_{vib}) and rotational inertia (I^1_{rot}) as a function of ε', where

$$\varepsilon' = \begin{cases} \varepsilon & \text{for the prolate shape} \\ i\varepsilon & \text{for the oblate shape} . \end{cases}$$

$$I_{vib} = I_0 \frac{2}{9} \frac{\varepsilon^2(3 - \varepsilon^2)}{(1 - \varepsilon^2)^{8/3}} ,$$

$$I^1_{rot} = I_0 \frac{2 - \varepsilon^2}{(1 - \varepsilon^2)^{2/3}} , \qquad I_0 = \frac{1}{5} A R_0^2 ,$$

where A is the mass of target nucleus whose radius is R_0.

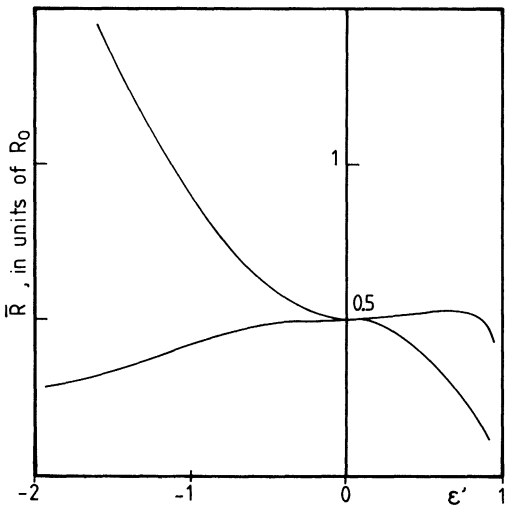

Fig. 1-2. — Two extreme values of the mean curvature $\overline{R}$ as a function of ε'.

The surface of the spheroidal target nucleus, its curvature, its self-Coulomb energies (V_d) and the moments of inertia are calculated from reference [6].

The equations of motion are

$$\frac{d}{dt} \frac{\partial}{\partial \dot{q}} L - \frac{\partial}{\partial q} L = 0$$

for $q = r, \Theta, \Phi, \theta, \varphi, \psi, \varepsilon$.

The equations for $q = \psi, \varepsilon, \theta$ are briefly considered below :

i) $q = \psi$; this coordinate is cyclic. Its canonical momentum is chosen to be zero, i.e., $\dot{\varphi} \cos\theta + \dot{\psi} = 0$.

ii) $q = \varepsilon$

$$I_{vib}\,\ddot{\varepsilon} + \frac{1}{2}\dot{I}_{vib}\,\dot{\varepsilon} - \frac{\partial I^1_{rot}}{\partial \varepsilon}\,\frac{1}{2}(\dot{\theta}^2 + \dot{\varphi}^2 \sin^2\theta) + \frac{\partial V}{\partial \varepsilon} = 0 . \quad (2)$$

The third term of eq. (2) represents the coupling between rotation and vibration through the change of inertia.

iii) $q = \theta$

$$I^1_{rot}\,\ddot{\theta} + \dot{I}^1_{rot}\,\dot{\theta} - I^1_{rot}\,\dot{\varphi}^2 \sin\theta + \frac{\partial V}{\partial \theta} = 0 . \quad (3)$$

3. **Results and discussion.** — Calculations were performed for the system $^{63}Cu + {}^{197}Au$ with 443 MeV bombarding energy. The impact parameter b was changed from 2 to 6 fm, which corresponds to a change in orbital angular momentum from 67 $\hbar$ to 200 $\hbar$. At $t = -\infty$ we assume that ^{197}Au is slightly deformed with $\varepsilon = 0.1$. (In Bohr's deformation notation, $\beta = 0.03$), and its symmetry axis points toward the angles shown in figure 2.

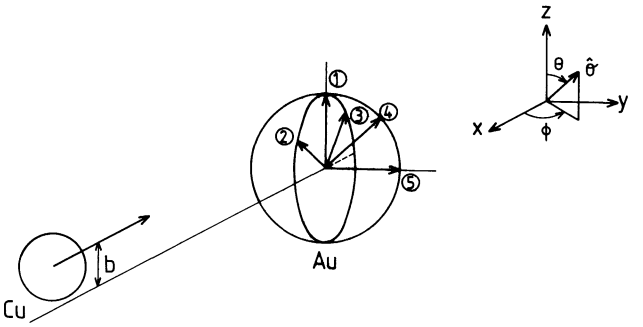

Fig. 2. — Geometrical orientation ($\hat{\sigma}$) of the symmetry axis of spheroidal nucleus (Au) is chosen to point toward different directions. b is the impact parameter. ① $\hat{\sigma} = (0, 0)$. ② $\hat{\sigma} = (\pi/4, 0)$. ③ $\hat{\sigma} = (\pi/4, \pi)$. ④ $\hat{\sigma} = (\pi/4, \pi/2)$. ⑤ $\sigma = (\pi/2, \pi/2)$.

In figure 3 the time evolution of the deformation, mass-vibrational energy, nuclear potential and orbital angular momentum for two different initial orientations, $\hat{\sigma}$, are shown; (a) $\hat{\sigma} = (0, 0)$, $b = 2$ fm; (b) $\hat{\sigma} = (\pi/4, 0)$, $b = 2$ fm.

$t = 0$ is taken when the distance between the two C.M. is 50 fm. The time unit is 10^{-21} second.

(I) The following remarks can be made concerning figure 3-1, where the deformation of ^{197}Au is shown as a function of time :

i) Until the nuclear interaction comes into play ($t \sim 1.0$), the Coulomb interaction causes Au to deform into two different shapes, one more prolate for case (a) and the other oblate (b);

ii) The deformation has no simple periodicity during the time in which the nuclear interaction takes place;

iii) The deformation in case (a) becomes pronounced in the exit channel ($t > 1.52$) but in case (b) this already happens in the entrance channel ($t < 1.64$);

iv) The resulting deformation in the exit channel will be prolate for both initial orientations.

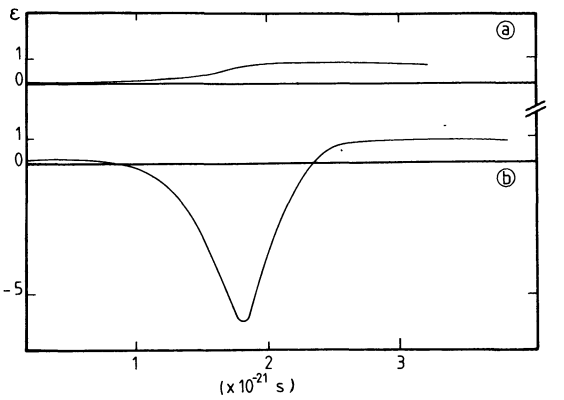

Fig. 3-1. — Time evolution for the deformation coordinate (ε). $t = 0$ is chosen when the relative distance is 50 fm.
(a) = $\hat{\sigma} = (0, 0)$, (b) = $\hat{\sigma} = (\pi/4, 0)$. Negative values of ε are for oblate deformation.

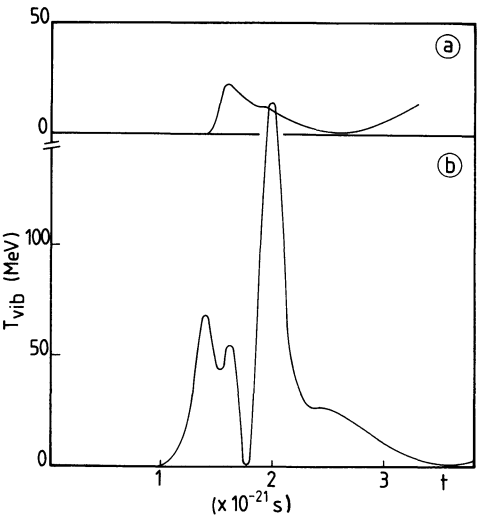

Fig. 3-2. — Same as figure 3-1 for vibrational energy (MeV).

(II) The following two remarks can be made concerning figure 3-2, where the vibrational energies of (a) and (b) are shown as a function of time :

i) The vibration mode in (a) is excited only in the exit channel but in (b) this occurs very early in the entrance channel.

ii) The vibrational energy in (a) is at most 25 MeV but in (b) it can be as great as 160 MeV. Such a high

vibrational energy value may be related to the fact that damping is neglected in our calculation. In the following paragraph the reason for these differences between (*a*) and (*b*) is given by simple derivation of the vibrational energy from the leading terms of eq. (2).

As mentioned, the third term of eq. (2) represents coupling between rotation and vibration. The ratio of the third to the second term of eq. (2) becomes

$$R = \left(\frac{\partial}{\partial \varepsilon} \log I^1_{\text{rot}} \Big/ \frac{\partial}{\partial \varepsilon} \log I_{\text{vib}} \right) (T_{\text{rot}}/T_{\text{vib}}) .$$

As shown in figure 1-1,

$$\frac{\frac{\partial}{\partial \varepsilon} \log I^1_{\text{rot}}}{\frac{\partial}{\partial \varepsilon} \log I_{\text{vib}}} \ll \frac{1}{10} . \qquad (4)$$

We can therefore ignore the third term unless the rotational energy is much higher than the vibrational energy, but comparison with figure 3-4 shows the smallness of R. A simple calculation to obtain the explicit appearance of I_{vib}, gives

$$T_{\text{vib}} \simeq \frac{1}{2} \int^t \mathrm{d}t' \int^t \mathrm{d}t'' \frac{I}{(I_{\text{vib}}(t')\, I_{\text{vib}}(t''))^{1/2}} \times \times \frac{\partial V}{\partial \varepsilon}(t') \frac{\partial V}{\partial \varepsilon}(t'') \qquad (5)$$

T_{vib} depends principally on two parameters : I_{vib} and $\partial V/\partial \varepsilon$.

Once the nuclear potential V_{N} intervenes this governs the movements. It is thus sufficient to consider $\partial V_{\text{N}}/\partial \varepsilon$ instead of $\partial V/\partial \varepsilon$.

i) At the moment when V_{N} begins to interact, Au in (*a*) is deformed with $\varepsilon \simeq 0.2$ but in (*b*) with $\varepsilon \simeq -0.9$.

This deformation difference signifies a large possible difference in $\partial V_{\text{N}}/\partial \varepsilon$, as can be easily deduced from figure 1-2. Since the proximity nuclear potential is linearly proportional to the mean curvature, $\overline{R}$, $\partial V_{\text{N}}/\partial \varepsilon$ is simply proportional to the tangent of the curves shown in figure 1-2.

ii) For the prolate nucleus, the increase in $\partial V_{\text{N}}/\partial \varepsilon$ is compensated by the increase in I_{vib}, this latter rising quite quickly above $\varepsilon \simeq 0.5$. Vibrational energy in (*b*) therefore reaches a maximum at fairly small deformation.

(III) We observe by comparison between figure 3-2 and figure 3-4 that the vibration mode acquires much more energy than the rotation mode. This difference can be explained in almost the same way as in the previous paragraph but with an additional restriction on time, i.e. $t < 1.6$.

The ratio between the second and fourth terms of eq. (3) leads to

$$R = \left(\frac{\partial}{\partial t} \log I^1_{\text{rot}} \right) . (J/(\partial V_{\text{N}}/\partial \theta)) ,$$

where $J = I^1_{\text{rot}}\, \dot{\theta}$ is the spin angular momentum of Au.

In the limit of $t < 1.6$, $\dot{\varepsilon}$ becomes small when $\partial I_{\text{rot}}/\partial \varepsilon$ increases and *vice versa*, which means that $\partial I_{\text{rot}}/\partial t$ is small. The same applies to the spin angular momentum, J.

We can therefore neglect the second term and consider that the rotational inertia is constant within the above time limits. Eq. (3) gives

$$T_{\text{rot}} \simeq \frac{1}{2\, I^1_{\text{rot}}} \int^t \mathrm{d}t' \int^t \mathrm{d}t'' \frac{\partial V}{\partial \theta}(t') \frac{\partial V}{\partial \theta}(t'') .$$

The influence of I^1_{rot} and of I_{vib} on energy is revealed in the above equation and in eq. (5). T_{vib} could be higher than T_{rot} by a factor of 10 because of the inertia difference.

(IV) The proximity nuclear potential, V_{N}, is shown as a function of time in figure 3-3.

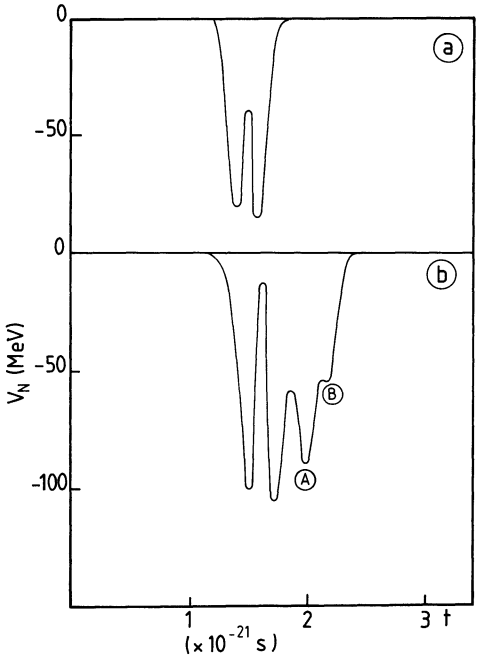

Fig. 3-3. — Same as figure 3-1 for nuclear proximity potential (MeV).

For case (*a*), two nuclei approach until a strong repulsive core is met then they separate. The same procedure is taken for case (*b*) until the target nucleus Au is quite deformed ($t \simeq 1.8$). Transformation of the deformation energy into vibrational and rotational energy induces a relatively rapid surface movement while the relative kinetic energy is low. Continuation of nuclear surface movement in the proximity of the other nuclear surface results in a new attractive interaction. (Ⓐ in the figure.) A similar situation can be shown to exist around $t = 2.2$ (Ⓑ in the figure), but the radial kinetic energy already becomes

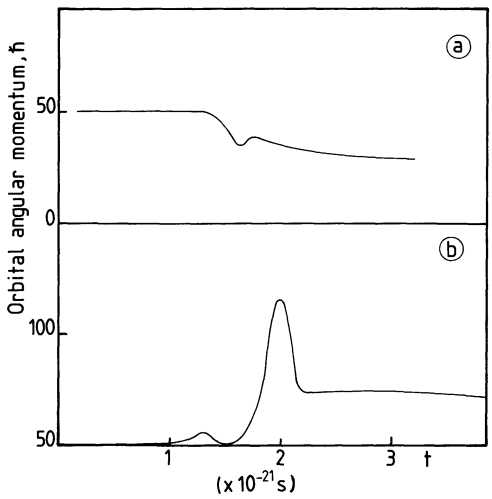

Fig. 3-4. — Same as figure 3-1 for orbital angular momentum ($\hbar$).

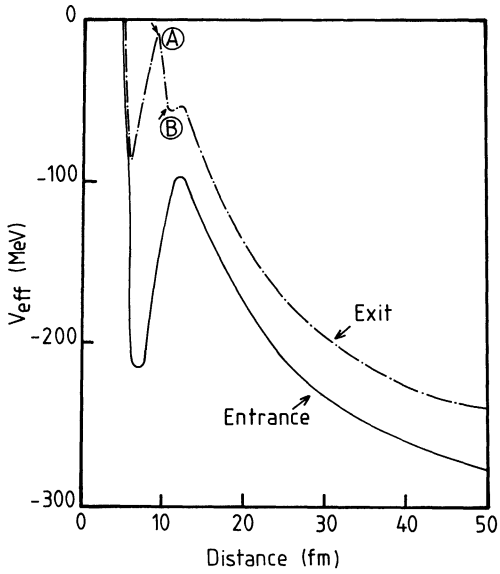

Fig. 4. — Effective potential energy (V_{eff}) which is the difference between total energy and radial kinetic energy, as a function of relative distance (fm). The solid line refers to the entrance channel and the dashed line to the exit channel. Almost 40 MeV of kinetic energy is transformed into deformation energy. Zero of V_{eff} is chosen arbitrary. Ⓐ and Ⓑ indicate the moments shown in figure 3-3.

55 MeV (see Fig. 4). Hence the nuclear potential does not show the pronounced local minimum observed at $t = 2.0$.

(V) The change of orbital angular momentum is shown in figure 3-4.

The spin angular momentum (J) of Au is the difference between each value of orbital angular momentum and the initial value. The corresponding rotational energy of Au can be easily calculated from the rigid body relationship between angular momentum and rotational energy. For example,

$$T_{\text{rot}} = 2.0 \text{ MeV} \quad \text{for} \quad \varepsilon = -5.5, \qquad J = 23\ \hbar$$

$$T_{\text{rot}} = 1.4 \text{ MeV} \quad \text{for} \quad \varepsilon = 0.93, \qquad J = 23\ \hbar.$$

The final changes in quantity of angular momentum are almost 20 $\hbar$, coming from the variations of the shape and of the orientation of the target nucleus. However these changes manifest themselves by opposite signs, i.e., the induced angular momentum of the deformed nucleus has the same direction as the orbital angular momentum for case (*a*) but the opposite direction for case (*b*). This 40 $\hbar$ difference results in a large dispersion in angular distribution shown in figure 5.

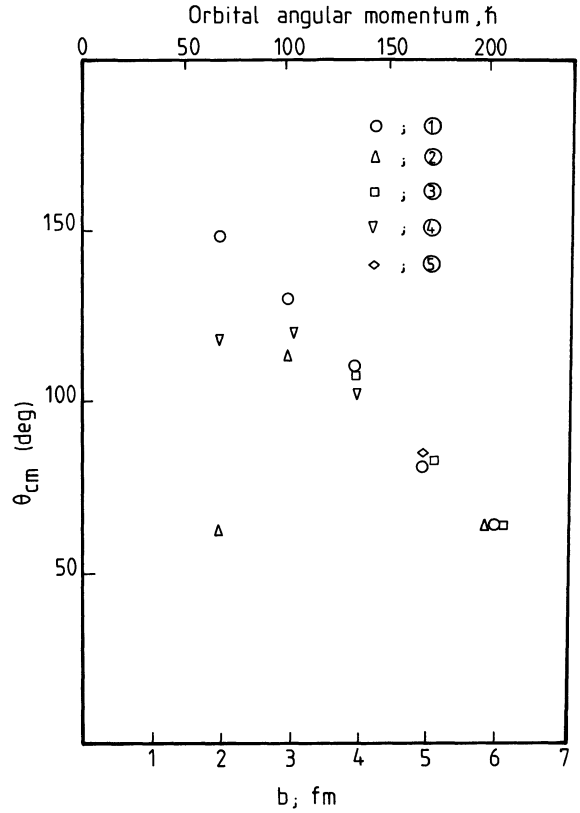

Fig. 5. — C.M. angular distribution for given impact parameters and symmetry axis orientations. The orbital angular momenta are also shown. For different orientation, see figure 2.

(VI) In figure 5 the deflection function is drawn for different symmetry axis orientations showing that not only the statistical equilibration but also the orientation of the deformed nucleus can be responsible for the dispersion on the Wilczynski diagram. The reduced dispersion found at large impact parameters is due to the absence of deformation in the entrance channel in these cases.

(VII) For cases where there is no spatial symmetry, like case 3 in figure 2 ($b = 5$ fm), we observe in figure 6 the large deviation of the spin direction for the deformed nucleus. In the centre of mass system, for example the relative vector is $\mathbf{r} = (50, 95.9, 90)$ in the entrance channel but $\mathbf{r} = (55.9, 173.5, -60)$ in the exit channel as shown in the figure. It is therefore incorrect to say that the initial direction of orbital angular momentum

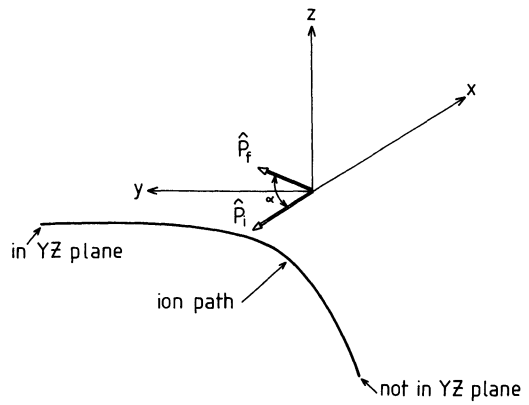

Fig. 6. — $\hat{P}_f$ represents the normal direction vector to the so called *reaction plane* defined by the plane of the ion path, not in *yz* plane. $\hat{P}_i$ represents the initial direction of orbital angular momentum. Angle, α, between $\hat{P}_i$ and $\hat{P}_f$ is almost 10°.

is perpendicular to the, so called, reaction plane defined by the plane of the ion path. This direction ($\hat{P}_f$) perpendicular to the reaction plane deviates from the true initial direction which is $\hat{P}_i$.

As a result the acquired spin of the deformed nucleus is likewise not oriented along $\hat{P}_f$. This phenomenon is also true for cases where a large deformation occurs, as usually happens when the impact parameter is small.

For the above mentioned case (case 3 in figure 2 with $b = 5$ fm), the ratio between the spin component of the spheroidal nucleus parallel to $\hat{P}_f$ and the spin component normal to $\hat{P}_f$ is as low as 0.6, from which we deduce the classical value of the spin projection to $\hat{P}_f$ axis, M_i,

$$M_i \simeq 6\,\hbar \quad \text{for} \quad J_i = 12\,\hbar$$

using the angular distribution formula for the quadrupole gamma ray, emitted when the nucleus decays from the state $| J_i, M_i \rangle$ to the state $| J_f, M_f \rangle$.

$$W(\sigma) = | \langle J_i, M_i, 2, M_i - M_f | J_f, M_f \rangle |^2 \times \times | Y_{2,2,1}^{M_i - M_f}(\sigma) |^2$$

where σ is the azimuthal angle from $\hat{P}_f$ axis, $\langle | \rangle$ is usual Clebsch-Gordon coefficient, and Y are usual spherical vector harmonics, we find

$$\frac{W(0)}{W(\pi/2)} = 0.8 \quad \text{for} \quad J_f = J_i - 2$$

instead of zero if the spin was aligned with $\hat{P}_f$. This is in reasonable agreement with the experimental value which is about 0.9 [2].

In conclusion, this de-orientation effect due to the dynamics is much more important than the de-orientation effect due to the emission of light evaporated particles. It becomes possible to explain the unexpected isotropic distribution of gamma rays discussed as above, and the anomalous angular distribution of the fission fragments, when the fissioning nucleus is a deep inelastic reaction product [8].

Likewise the Coriolis effect must align the spin of the deformed nucleus into the $\hat{P}_i$ direction but not into the $\hat{P}_f$ direction.

Acknowledgments. — The author is very grateful to M. Martinot for stimulating discussions and encouragement during this work.

References

[1] Deubler, H. H. and Dietrich, K., *Nucl. Phys.* A **277** (1977) 493 ; *Phys. Lett.* **69B** (1977) 137 ; *Phys. Lett.* **56B** (1975) 241.
Bondorf, J. P., Sobel, M. I. and Sperber, D., *Phys. Lett. Rep.* **15C** (1975).
Nix, J. R. and Sierk, A. J., *Phys. Scr.* **10A** (1974) 401.
Gross, D. H. E. and Kalinowski, H., *Phys. Lett.* **48B** (1974) 302.
Tsang, C. F., *Phys. Scr.* **10A** (1974) 90.
Siwek-Wilczynska, K. and Wilczynski, J., *Nucl. Phys.* A **264** (1976) 115.
Bass, R., *Nucl. Phys.* A **231** (1974) 45.
Bondorf, J. B., Huizenga, J. R., Sobel, M. I. and Sperber, D., *Phys. Rev.* C **11** (1975) 1265.
Ngo, C. and Hofmann, H., *Z. Phys.* A **282** (1977) 83.
[2] Berlanger, M. *et al.*, *J. Physique Lett.* **37**(1976) L-323.
Simon, R. S. *et al.*, *Phys. Rev. Lett.* **36** (1976) 357.
[3] Randrup, J., Swiatecki, W. J. and Tsang, C. F., LBL report (1974) 3603.
Błocki, J., Randrup, J., Swiatecki, W. J. and Tsang, C. F., *Ann. Phys.* **105** (1977) 427.
[4] Randrup, J., NORDITA 78/9.
[5] Morse, P. M. and Fesbach, M., *Methods of Theoretical Physics* (Mc Graw-Hill) 1953, p. 1291.
[6] Pal, M. K., IAEA report, Miramore-Trieste, IC/71/42.
[7] Beringer, R. and Knox, W. J., *Phys. Rev.* **4, 121** (1961) 1195.
Kan, K. K. and Griffin, J. J., *Nucl. Phys.* A **301** (1978) 258.
[8] Back, B. B. and Bjornhorm, S., *Nucl. Phys.* A **302** (1978) 343.